DC reactive magnetron sputtering, annealing, and characterization of CuAlO2 thin films

Blake L. Stevens, Cathleen A. Hoel, Carolyn Swanborg, Yang Tang, Chuanle Zhou et al.

Related Articles

Atomic layer deposition of Al-doped ZnO thin films
J. Vac. Sci. Technol. A 31, 01A109 (2013)

Band alignment of zinc oxide as a channel layer in a gate stack structure grown by plasma enhanced atomic layer deposition
J. Vac. Sci. Technol. B 30, 051807 (2012)

Thin InAs membranes and GaSb buffer layers on GaAs(001) substrates
J. Vac. Sci. Technol. B 30, 051202 (2012)

Biaxial texture development in aluminum nitride layers during off-axis sputter deposition
J. Vac. Sci. Technol. A 30, 051501 (2012)

Indium and impurity incorporation in InGaN films on polar, nonpolar, and semipolar GaN orientations grown by ammonia molecular beam epitaxy
J. Vac. Sci. Technol. A 30, 041513 (2012)

Additional information on J. Vac. Sci. Technol. A

Journal Homepage: http://avspublications.org/jvsta

Journal Information: http://avspublications.org/jvsta/about/about_the_journal

Top downloads: http://avspublications.org/jvsta/top_20_most_downloaded

Information for Authors: http://avspublications.org/jvsta/authors/information_for_contributors

DC reactive magnetron sputtering, annealing, and characterization of CuAlO$_2$ thin films

Blake L. Stevens[a)]
Department of Materials Science and Engineering, Northwestern University, Evanston, Illinois 60208

Cathleen A. Hoel
Department of Chemistry, Northwestern University, Evanston, Illinois 60208

Carolyn Swanborg
Department of Materials Science and Engineering, Northwestern University, Evanston, Illinois 60208

Yang Tang, Chuanle Zhou, and Matthew Grayson
Electrical Engineering and Computer Science, Northwestern University, Evanston, Illinois 60208

Kenneth R. Poeppelmeier
Department of Chemistry, Northwestern University, Evanston, Illinois 60208

Scott A. Barnett
Department of Materials Science and Engineering, Northwestern University, Evanston, Illinois 60208

CuAlO$_x$ thin films were prepared at three substrate temperatures (T_S=60, 300, and 600 °C) and two oxygen partial pressures (P_{O_2}=0.5 and 2 mTorr) via dc reactive magnetron sputtering from Cu–Al 50–50 at. % alloy targets and subsequent annealing. As-deposited films with P_{O_2}=0.5 mTorr were oxygen deficient; although the delafossite structure formed upon annealing, electrical properties were poor. Films deposited with P_{O_2}=2 mTorr transformed into the delafossite structure and exhibited p-type conductivity after annealing under N$_2$ at temperatures $T_A \geq 750$ °C. Conductivity generally increased with increasing T_S and decreasing T_A. A special case of P_{O_2}=2 mTorr and low T_S (60 °C) resulted in a partially crystalline oxide phase that transformed into the delafossite structure at T_A=700 °C and yielded the highest conductivity of 1.8 S cm^{-1}. In general, a T_A near the phase formation boundary led to an increase in conductivity. Low-temperature hydrothermal annealing was also investigated and shown to produce mixed phase films exhibiting the delafossite structure along with CuO, AlOOH, and Al$_2$O$_3$. © *2011 American Vacuum Society.*
[DOI: 10.1116/1.3525640]

I. INTRODUCTION

Transparent conducting oxides (TCOs) have many technological uses, including flat panel displays, photovoltaics, and low emissivity window glass.[1] Almost all TCOs are n-type semiconductors, but there has been considerable interest in p-type TCOs, which would have applications in transparent electronics, functional windows, and transparent complementary field-effect transistors.[2] Of the few transparent oxide materials exhibiting p-type conductivity, a number are from a class of delafossite structure oxides epitomized by CuAlO$_2$.[3] This ABO$_2$ crystal structure consists of alternating layers of B^{3+}O$_6$ octahedra and closest packed, linearly coordinated A^{1+} cations.[4]

Since the initial report of laser ablated CuAlO$_2$ thin films exhibiting p-type conductivity,[3] p-type delafossite structure CuAlO$_2$ has been synthesized by various methods including rf sputtering[5–7] and dc sputtering.[8–10] Sputter deposition is of particular interest because it is widely used in industry for depositing TCOs.[11] Two strategies have been employed to yield the delafossite phase in sputtered films, namely, direct deposition and deposition followed by annealing. Direct delafossite formation has been reported in a few cases, using both oxide and metallic targets, but conductivities were relatively low, 0.08–0.51 S cm^{-1}.[8,9,12] In other cases a post-deposition annealing in an inert atmosphere (Ar or N$_2$) was required to transform the films into the delafossite structure. In a case where films with varying Cu:Al ratios were obtained by reactively sputtering from separate Cu and Al targets, annealing at temperature $T_A > 700$ °C was necessary to form the delafossite structure, and a maximum conductivity of ~0.1 S/cm was observed.[10,13] For films sputtered from a single Cu–Al alloy target, the delafossite structure was obtained at $T_A > 600$ °C and conductivity (0.038 S cm^{-1}) was observed only for annealing at $T_A > 800$ °C.[14]

This article describes films reactively sputtered from a single Cu–Al alloy target at various temperatures and the effects of postdeposition annealing conditions on their phase formation, crystal structure, morphology, electrical properties, and optical properties. The main aim of the work was to provide a clearer picture of the phase evolution and electrical properties upon annealing at different T_A, and the role of deposition conditions including oxygen partial pressure and temperature. Through studying this process, the path to the highest reported conductivity of CuAlO$_2$ films via physical

---

a)Electronic mail: b-stevens@u.northwestern.edu

vapor deposition was discovered, $\sigma = 1.83$ S/cm. Also, initial results on hydrothermal annealing, with the potential to form the delafossite structure at lower temperature than possible using conventional annealing, are presented.

II. EXPERIMENTAL DETAILS

Cu–Al–O films were deposited via dc reactive magnetron sputtering in a load-locked vacuum system, described elsewhere.[15] A metallic 50–50 at. % Cu–Al target of 99.99% purity was used for all of the depositions. The target to substrate distance was ~14 cm. The target was kept at a constant power of 100 W throughout the depositions.

The chamber was evacuated to a pressure of $P_{tot} < 3.0 \times 10^{-7}$ Torr, after which a mixture of argon and oxygen was leaked into the system via mass flow controllers to attain a total pressure of $P_{tot} = 5.0$ mTorr. The oxygen partial pressure was either $P_{O_2} = 0.5$ mTorr (10% oxygen) or 2.0 mTorr (40% oxygen). The substrates used in this study were single crystal *c*-plane sapphire. Prior to loading into the deposition chamber, the wafers were ultrasonically cleaned in acetone and methanol for 10 min each. The substrates were further cleaned in the chamber by heating to 600 °C for at least 30 min. The substrate temperature, T_S, during deposition, ~60 °C (no intentional heating), 300 °C, or 600 °C, was controlled via a resistively heated silicon wafer.

The composition of several as-deposited films was determined by inductively coupled plasma atomic emission (ICP-AES, Varian Vista-MPX). The films were placed in 5 ml of 5% aqua regia (by volume) in a Parr pressure vessel lined with a 23 ml Teflon polytetrafluoroethylene (PTFE) cup. After 12 h of digestion at 150 °C, no visible trace of film was left on the substrate. The Cu:Al ratio of the final solution was measured. A blank sapphire substrate was also digested by the same procedure to correct for Al that dissolved from the substrate.

Two different atmospheric annealing procedures were used in this study. The samples deposited with $P_{O_2} = 0.5$ mTorr underwent a two-step annealing, the first at moderate temperature (500–700 °C) in air with a subsequent annealing at elevated temperature (650–900 °C) under N$_2$. Samples deposited with $P_{O_2} = 2$ mTorr only required the second annealing step. For these films, a series of annealing was completed from 650 to 900 °C in 50 °C increments under N$_2$. In all annealing, the temperature was ramped to the annealing temperature at a rate of 5°/min, maintained at the hold temperature for 6 h, and then cooled. Prior to the annealing process, the furnace tube was purged with nitrogen for a minimum of 12 h.

Investigations of the effects of hydrothermal annealing were also completed on the films. Hydrothermal annealing has previously been used successfully to produce highly crystalline films of Zn$_2$SiO$_4$, ZrO$_2$, and MnO$_2$ from films that had been deposited in an amorphous state by successive ionic layer adsorption and reaction.[16] The films were placed in a Parr pressure vessel lined with 23 ml Teflon PTFE cups with 0.05–0.30 ml water. The pressure vessel was heated to a maximum of 250 °C, at which point elevated vapor pressures of 5–15 atm were obtained. Similar temperature and pressure conditions have previously been used to hydrothermally synthesize bulk CuAlO$_2$ powders.[4] Several films were hydrothermally annealed at 300 °C. These films and 2.0 ml water were heated in a 300 ml stainless steel Parr pressure vessel fitted with a PTFE-flat gasket. Both 0.5 and 2.0 mTorr P_{O_2} films were investigated. Annealing times varied from 6 to 24 h. To prevent excessive oxidation of the film from atmospheric O$_2$, the water was preboiled and the films were loaded and sealed in the pressure vessels under N$_2$.

Films were characterized with grazing incidence x-ray diffraction (XRD) using a Rigaku ATX-G diffractometer and 2θ-θ x-ray scans using a Rigaku RU-200PL diffractometer. Films were also examined by atomic force microscopy (AFM, Nanoscope) to determine surface roughness. Film thickness was measured with a Tencor P10 surface profilometer.

Annealed films that showed a predominantly delafossite phase by XRD underwent electrical measurements (BioRad HL5500 and hot-probe device) and optical measurements for band gap and transparency (Cary 500 scan UV-VIS-NIR). Selected samples were also examined with scanning electron microscopy (SEM, Hitachi S-4800-II microscope).

Due to the high resistivity and high carrier concentration of the samples, Hall measurements in standard $B = 0.3$ T tabletop magnets may not be reliable. Thus for Hall measurements, a superconducting 15 T magnet was used with a helium flow cryostat operating at 300 K. Van der Pauw measurements of high resistivity samples inevitably mix a component of the longitudinal resistance R_{xx} with the Hall signal R_{xy}. Since thermal fluctuations of order of 0.5 K cannot be avoided, the large thermal coefficient of R_{xx} results in drifting signals that can overwhelm the small Hall signal. To eliminate this effect, a scaled component of the simultaneously measured longitudinal resistance is subtracted from the Hall measurement to yield a pure R_{xy} trace. Best results were obtained by difference averaging $R_{xy}(+B)$ up sweep with $R_{xy}(-B)$ down sweep. By averaging 36 Hall measurement sweeps to 15 T, the noise was reduced enough to determine a Hall coefficient.

Temperature dependent electrical measurements were completed on select films using an Oxford variable temperature insert helium flow cryostat from 300 to 80 K. Standard lock-in techniques at 2.125 Hz measured both the current and the four-point voltage under a $V_{ac} = 0.6$ V excitation. Van der Pauw four-point conductivities at 300 and 250 K were used to calibrate the two-point conductivity versus temperature curve.

III. RESULTS AND DISCUSSION

A. As-deposited films

The composition of the films was verified to be 1:1 Cu:Al by ICP-AES. This composition agrees with that of the sputtering target, indicating that the sputtering was carried out under a steady state condition. A deposition time was chosen to create 200–300 nm thick films, as verified by profilometry.
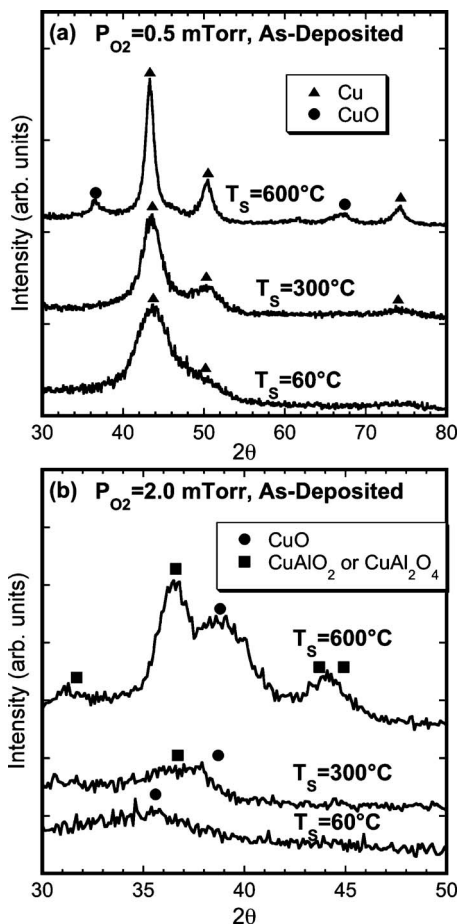
FIG. 1. Grazing incidence XRD scans from Cu–Al–O films deposited at (a) P_{O_2}=0.5 mTorr and (b) P_{O_2}=2 mTorr, and substrate temperatures of 60, 300, and 600 °C. Peak positions expected for various phases are marked with different symbols as indicated.

Initial experiments were done varying the oxygen partial pressure P_{O_2} during the sputter deposition with the total Ar +O_2 pressure maintained constant. The target voltage remained relatively constant with increasing P_{O_2} up to $\approx$0.8 mTorr (15% of total pressure). For P_{O_2} increased above 0.8 mTorr, there was a large voltage drop, implying target surface oxidation.[17] The target was believed to be fully poisoned at pressures greater than 0.8 mTorr. The sputter deposition rate decreased with increasing P_{O_2}, e.g., going from $\sim$230 nm/min in pure Ar to 15 nm/min at P_{O_2}=0.5 mTorr, to 0.5 nm/min at P_{O_2}=0.8 mTorr, and finally to $\sim$0.3 nm/min at P_{O_2}=2 mTorr P_{O_2}.

Films deposited with P_{O_2}<0.8 mTorr were not fully oxidized. Figure 1(a) shows an example of grazing incidence XRD scans from depositions with P_{O_2}=0.5 mTorr at three different substrate temperatures T_S. A number of strong peaks were present that indexed to metallic Cu indicating that the films were not fully oxidized. Amorphous alumina may have been present, but was not obvious in the XRD scans. At the highest T_S, 600 °C, some CuO was detected.

These films all had a dark brown/black coloration and were not transparent to visible light, consistent with the conclusion that they were not fully oxidized.

Increasing P_{O_2} yielded increasingly oxidized films, with the films becoming visually transparent for P_{O_2}>1 mTorr. Figure 1(b) shows the XRD scans from films grown with P_{O_2}=2 mTorr, typical of fully oxidized films. The crystallinity of the films was dependent on T_S. While the T_S $\sim$60 °C films had little observable structure, peaks were observed at higher T_S that indexed to various oxide phases, including CuO and CuAl$_2$O$_4$, indicating that the films were fully oxidized. At no point was delafossite CuAlO$_2$ observed in as-deposited films. This lack of a delafossite phase agrees with prior reports for films deposited under similar conditions,[10,14] where it was found that delafossite formation required $T_S \geq$700 °C, higher temperatures than used in the present study.

Surface roughness, as measured by AFM, increased with increasing T_S. Films deposited at $\sim$60 °C had smooth surfaces with rms roughness of $\sim$0.2 nm. Films deposited with T_S=300 and 600 °C had rms roughness values of 0.5 and 2.2 nm, respectively.

B. Ambient-pressure annealed films

1. Structure of films deposited with low P_{O_2}

Given that the films deposited at P_{O_2}=0.5 mTorr were partially metallic, it was required that the annealing procedure should also oxidize the films. A variety of single-step oxidizing annealing procedures were attempted, but none of these yielded delafossite phase films. A two-step annealing process was thus used, namely, an annealing at temperature T_A=500–700 °C in air and followed by an annealing at higher temperatures (T_A=700–900 °C) under nitrogen flowing at 50 SCCM (SCCM denotes cubic centimeter per minute at STP). An example of the structural evolution can be seen in the XRD scans in Fig. 2. Under the air annealing, the partially metallic as-deposited film was fully oxidized, exhibiting CuO peaks in XRD with no metallic Cu present. The film then formed the delafossite phase during a reducing annealing at 900 °C in N$_2$.

While the two-step annealed films exhibited the desired delafossite structure, their properties were not ideal. First, the films had high surface roughness (50 nm rms). Second, the conductivities were quite low with the highest measured at 0.02 S cm^{-1} and most films showing values too low to measure ($\sim$<0.01 S/cm). Thus, subsequent annealing studies were carried out using films deposited with P_{O_2}=2 mTorr.

2. Structure of films deposited with high P_{O_2}

Films deposited with P_{O_2}=2 mTorr and either T_S=60, 300, or 600 °C were annealed in dry N$_2$ from T_A=650 to 900 °C. Relatively little change in structure resulted from annealing at T_A<650 °C with the XRD similar in appearance to that of the as-deposited films (Fig. 1). Figure 3(a) shows grazing incidence XRD data from $T_S \sim$60 °C films after annealing at three different temperatures. At T_A
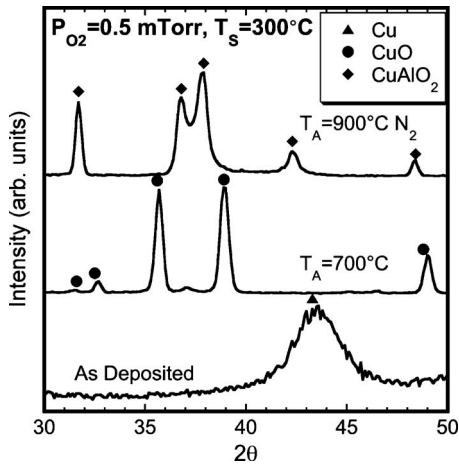
FIG. 2. Grazing incidence XRD scans from a film deposited with P_{O_2} =0.5 mTorr and a substrate temperature of 300 °C after annealing at 700 °C in air, and after a subsequent anneal at 900 °C in N_2. Peak positions expected for various phases are marked with different symbols as indicated. The peaks attributed to $CuAlO_2$ identify to (006), (101), (012), (104), and (009) from left to right.
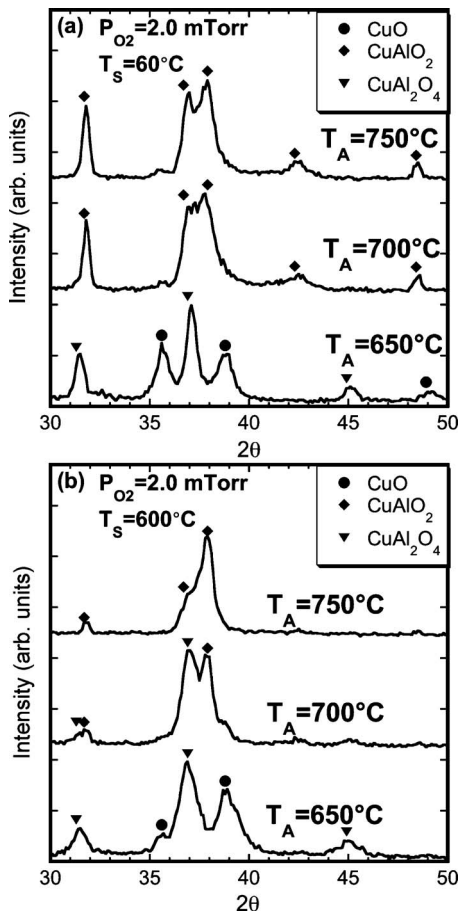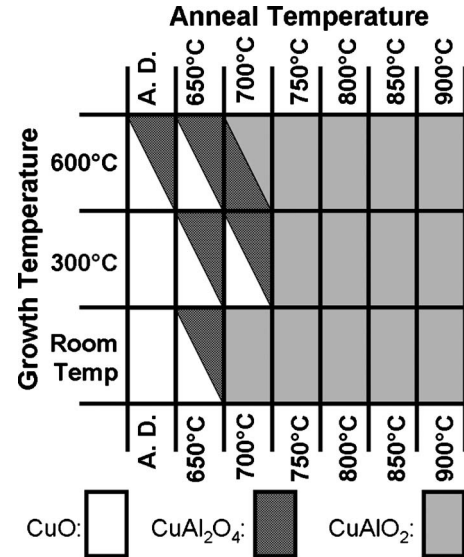

FIG. 4. Map of the phases present vs growth and annealing temperature in as-deposited and annealed films. Films were deposited with P_{O_2}=2 mTorr and annealed under N_2. CuO, $CuAl_2O_4$, and $CuAlO_2$ are represented by white, dark gray, and gray respectively.

FIG. 3. Grazing incidence XRD scans from Cu–Al–O films deposited at (a) 60 and (b) 600 °C with P_{O_2}=2 mTorr after annealing at different temperatures. Peak positions expected for various phases are marked with different symbols as indicated. The peaks attributed to $CuAlO_2$ identify to (006), (101), (012), (104), and (009) from left to right.

=650 °C, the films consisted of CuO, spinel $CuAl_2O_4$, and possibly amorphous alumina. At T_A=700, 750 °C, and above (not shown), the delafossite peaks dominated the XRD scans. Figure 3(b) shows grazing incidence XRD scans from films deposited at T_S=600 °C. The phases observed after annealing were similar to those for films deposited at T_S =60 °C, but formation of the delafossite phase was delayed until $T_A \approx 750$ °C. It is perhaps reasonable that the delafossite phase appeared only at higher T_A in the films deposited at higher T_S because it may have been more difficult for the delafossite phase to replace crystalline phases that were already well-established prior to annealing. A similar delay of delafossite formation was also seen in the films grown at 300 °C. Annealing temperatures at or above 750 °C were sufficient to produce the delafossite structure, as measured by XRD for all T_S.

Figure 4 summarizes the above results in a map of the phases present versus T_A and T_S. T_A had the strongest effect on the phases observed. As-deposited films showed CuO and $CuAl_2O_4$ at higher T_S. Films annealed at 650 °C exhibited mixed phases, predominantly CuO, $CuAl_2O_4$, and presumably some amorphous alumina. For $T_A \geq 700$ °C, a mixture of phases containing $CuAl_2O_4$ and delafossite was present, with the delafossite phase becoming dominant as T_A increased. The films appeared to be phase-pure delafossite to the detection limit of the XRD measurements for T_A ≥ 750 °C and also for T_A=700 °C for $T_S \sim 60$ °C. While time-dependent annealing experiments were not carried out, it seems likely that the transformation to the delafossite structure occurred via the spinel phase as an intermediate, as suggested previously,[18]
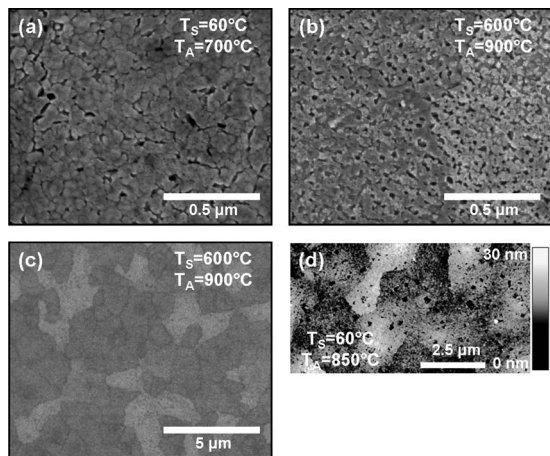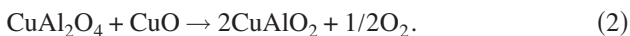
$$CuO + Al_2O_3 \rightarrow CuAl_2O_4, \qquad (1)$$

FIG. 5. (a) SEM image of a CuAlO$_2$ film with $T_S = 60$ °C and $T_A = 700$ °C. [(b) and (c)] SEM images of a CuAlO$_2$ film with $T_S = 600$ °C and $T_A = 900$ °C. (d) AFM image of CuAlO$_2$ film with $T_S = 60$ °C and $T_A = 850$ °C.

$$CuAl_2O_4 + CuO \rightarrow 2CuAlO_2 + 1/2O_2. \qquad (2)$$

Oxygen generation in the second reaction indicates that a reducing atmosphere should promote delafossite formation, which was observed in previous reports.[10,13,14] An equilibrium stability diagram at 1000 °C showed that the delafossite structure forms at low $P_{O_2} = 0.05$ mTorr up to atmospheric conditions.[19,20]

All films that fully transformed into the delafossite structure shared some common structural characteristics. The 2θ-θ x-ray scans (not shown) indicated a (001) preferred out-of-plane orientation, although weaker (101) and (012) peaks were also present. This preferred orientation agrees with prior work.[3,21] In general, a higher T_S led to a stronger (001) orientation based on the peak intensity ratios between (001) and (101) or (012). The degree of orientation cannot be seen in the grazing incidence XRD data presented in Figs. 2 and 3.

Grain sizes were calculated from the 2θ-θ XRD scans using Scherrer's formula and were found to vary between 60 and 110 nm. In general, high T_S and low T_A resulted in the smallest grain sizes, with the largest grains coming from 60 °C deposition and 900 °C anneal. The films did not show an epitaxial orientation relative to the sapphire substrate as tested by x-ray Φ scans.

After annealing, film surface rms roughness measured by AFM ranged from 2–4 nm, with no clear dependence on deposition conditions. This represented an increase in film surface roughness after annealing compared with the as-deposited roughness of 0.2 to 2.2 nm (see Sec. III A). The increase was most noticeable for low T_S films that had low as-deposited roughness values. In films annealed at ≤ 800 °C, only a small-scale (submicrometer) lateral surface morphology was present, as seen in Fig. 5(a). These submicrometer features are believed to be the grains and match well with the calculated grain size. Films annealed at $T_A \geq 850$ °C had a second, larger-scale surface structure. Figure 5(b) shows a SEM micrograph of these features, with a lower
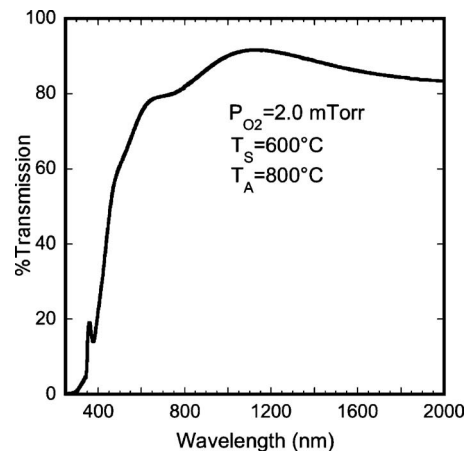

FIG. 6. Typical optical transmission vs wavelength data from a delafossite film deposited at 600 °C and annealed at 800 °C.

magnification seen in Fig. 5(c). As shown in the AFM image in Fig. 5(d), large plateaus with a height of ~ 5–10 nm were apparent. The larger-scale morphological features were not related to any compositional nonuniformity across the film, as verified by SEM-energy dispersive x-ray spectroscopy. The contrast differences of these features, shown in Figs. 5(b) and 5(c), are instead attributed to orientation variation across the sample. This variation could be caused by slight angular differences of the surface normal, such as those observed in AFM [Fig. 5(d)], or by long-range ordering among the submicrometer grains.

The submicrometer column/void structure is similar to prior observations on Cu–Al–O films annealed at 800 and 900 °C.[14] The mosaic structure was attributed to recrystallization of the films. The smaller voids could be attributed to shrinkage during crystallization coupled with the release of O$_2$ gas when the phases transformed from the initial amorphous Al$_2$O$_3$–CuO to crystalline CuAlO$_2$. When undergoing the transformation from a mixture of CuAl$_2$O$_4$+CuO to 2CuAlO$_2$, the average unit cell molar volume decreases by 7.5%. There is also expected to be an increase in density when going from an amorphous structure to a crystalline structure.[22–24]

C. Delafossite film properties

This section deals only with the annealed films deposited with $P_{O_2} = 2$ mTorr described above that showed predominantly the delafossite structure.

Figure 6 shows a typical result of optical transmission measurements. The highest transparency measured at 550 nm was in films deposited at 600 °C, with the highest percent transmission of 75% after an 850 °C annealing for a film 185 nm thick. The band gaps of the films were derived by fitting the linear portion of the absorption spectra.[25] Most films had calculated band gap values between 3.5 and 3.9 eV with no clear trends with T_A. However, films deposited at $T_S = 600$ °C had band gap values ~ 0.1 eV higher than films grown at lower T_S. These values fall mostly in the range of previously reported band gaps of 3.5–3.75 eV.[8,10,14]
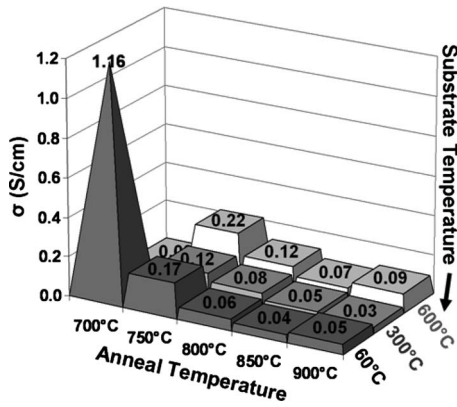
FIG. 7. Measured electrical conductivity (S cm^{-1}) of delafossite films vs their deposition T_S and annealing T_A temperatures.
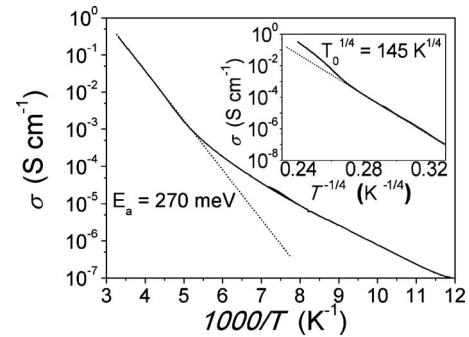

FIG. 8. Temperature dependence of conductivity σ vs reciprocal temperature T. Above 190 K, the conductivity follows the Arrhenius law $\sigma = \sigma_0 \exp(-E_a/k_B T)$ (fit shown) with an activation energy (E_a) of 270 meV. (Inset) Below 190 K, it follows the standard variable range hopping law $\sigma = \exp[-(T_0/T)^{1/4}]$ where $T_0^{1/4} = 145$ K$^{1/4}$.

All films in the delafossite structure exhibited p-type conductivity based on hot-probe measurements. This was also verified by the sign of the Hall coefficient during temperature dependent analysis. Figure 7 shows the results of electrical conductivity measurements on delafossite films versus T_S and T_A. The conductivity generally increased with decreasing T_A, with the $T_S = 60$ °C, $T_A = 700$ °C film showing by far the highest conductivity of 1.8 S/cm in a single sample with an average conductivity of 1.16 S/cm across multiple samples. This average value is comparable to the best reported conductivities for CuAlO$_2$ thin films grown by physical vapor deposition methods.[3] The present results show that the highest conductivity was achieved at the lowest T_A value that produced the delafossite phase. The dominant mechanism for p-type conduction in CuAlO$_2$ films is from the combination of O interstitials (O_i''), and Cu and Al vacancies (V_{Cu}' and V_{Al}'').[26] Oxygen vacancies, however, would have a detrimental impact on conductivity by compensating charge carriers in CuAlO$_2$ films that would decrease the conductivity. The lower annealing temperature allows for more O_i'' and fewer oxygen vacancies, which is consistent with the decreasing conductivity for higher annealing temperatures. The combination of the low substrate temperature, $T_S = 60$ °C, and high $P_{O_2} = 2$ mTorr yielded a mixture of as-deposited amorphous oxides. This initial microstructure formed the delafossite structure upon annealing with the most ease compared to the other as-deposited films that also contributed to the high conductivity.

Temperature dependent conductivity is shown in Fig. 8 for a film with $T_S = 60$ °C and $T_A = 700$ °C and a room temperature conductivity of $\sigma = 0.26$ S/cm. The Hall coefficient at room temperature was positive with a measured carrier concentration of 5×10^{19} cm^{-3}. The sample conductivity decreases as temperature decreases from 300 to 80 K. In the higher temperature range ($T > 190$ K), the conductivity obeys an Arrhenius activated behavior $\sigma = \exp(-E_a/k_B T)$ with activation energy $E_a = 270$ meV, slightly larger than the 200 meV activation of Kawazoe et al.,[3] but in line with the measurement by Banerjee et al. of 260 meV.[12] This value is far smaller than half of the band gap (~ 3.5 eV) as pointed out by Kawazoe et al.,[3] who interpreted E_a as the activation

energy from dopant band to valence band. Another possible interpretation is that E_a might correspond to activated hopping within the dopant band itself, in that case, the dopant binding energy could be significantly larger than E_a.[27] At lower temperature below ~ 190 K, the conductivity transitions to a variable range hopping law $\sigma = \exp[-(T_0/T)^{1/4}]$, as seen in the inset of Fig. 8, indicating that the Fermi energy is definitely within the doping band at these temperatures as pointed out in Ref. 3. The variable range hopping temperature scale is $T_0^{1/4} = 145$ K$^{1/4}$, comparable but somewhat larger than the value seen in the data of Ref. 3.

Hall measurements at room temperature show p-type conduction with a carrier density of the order $p = 5 \times 10^{19}$ cm^{-3} and Hall mobility of $\mu = 0.03$ cm^2/V s. This carrier density and mobility are comparable to Yanagi et al.,[28] but is more than two orders of magnitude larger than Kawazoe et al.,[3] suggesting that extra care may be required for reliable Hall data.

D. Hydrothermally annealed films

Films grown in both high (2 mTorr) and low (0.5 mTorr) P_{O_2} were studied using the hydrothermal annealing method. Films deposited at low P_{O_2}, which had a large concentration of metallic copper, were not robust enough to withstand the hydrothermal environment. During the annealing process, the films detached from the substrate. Therefore, further study was done for films deposited with $P_{O_2} = 2$ mTorr.

The films were observed by XRD after hydrothermal annealing at various times, temperatures, and vapor pressures. None of the films were phase-pure delafossite; they generally exhibited mixed phases of delafossite CuAlO$_2$, CuO, AlOOH (boehmite), and probably amorphous alumina. Figure 9 shows the XRD scans from films that exhibited the strongest delafossite phase peaks, for $T_S = 60$ and 300 °C, and annealing at 250 °C under ~ 12 atm water vapor for relatively long times. The following summarizes the effects of hydrothermal annealing temperature, pressure, and time on the observed phases. Films annealed at 150 °C for 12 h under ~ 12 atm remained amorphous. Films deposited with $T_S = 60$ and 300 °C and annealed at $T_A = 250$ and 300 °C for 12
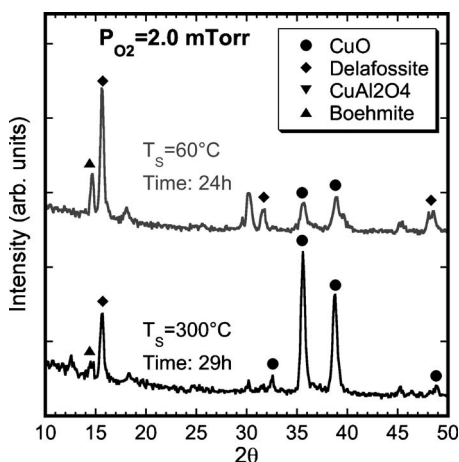
FIG. 9. Grazing incidence XRD scans from films hydrothermally annealed at 250 °C under 12 atm of water vapor. Peak positions expected for various phases are marked with different symbols as indicated. The peaks attributed to $CuAlO_2$ identify to (003), (006), and (009) from left to right.

or more hours and similar pressures showed crystalline phases including delafossite. Hydrothermal annealings with 0.05 ml water (~5 atm) showed no structural change, while annealings with 0.15 ml (~12 atm) and 3.0 ml water (~15 atm) did undergo a phase change at temperatures $T_A \geq 250$ °C.

IV. SUMMARY AND CONCLUSION

Thin films of delafossite $CuAlO_2$, a *p*-type TCO, were grown via dc reactive sputtering from an alloyed Cu–Al 50–50 at.% target and subsequent nitrogen-ambient annealing. The substrate temperature ($T_S=60$, 300, and 600 °C) oxygen partial pressure ($P_{O_2}=0.5$ and 2 mTorr) and annealing temperatures were explored to determine the conditions that led to delafossite formation. The trends in the film morphology and properties were also examined. Film surface roughness increased with increasing T_S. All $P_{O_2}=2$ mTorr films transformed into the delafossite phase for $T_A \geq 750$ °C, although films deposited at the lowest temperature, $T_S=60$ °C, transformed for $T_A \geq 700$ °C. The delafossite films exhibited (001) out-of-plane orientation, *p*-type conductivity, and band gaps of 3.5–3.9 eV. Electrical conductivity decreased with increasing annealing temperature. A room temperature deposited film annealed at 700 °C achieved a record conductivity of 1.8 S cm^{-1}. Temperature dependence shows activated conductivity above 190 K and variable range hopping at colder temperatures.

Hydrothermal annealing at 250 °C and 12 atm, starting with films deposited at $T_S \leq 300$ °C and $P_{O_2}=2$ mTorr, resulted in multiple phases including the delafossite structure, CuO, AlOOH, and Al_2O_3. Although single phase $CuAlO_2$

films were not obtained, with further study, hydrothermal annealing may provide a low-temperature route to phase-pure delafossite films.

[1]D. S. Ginley and C. Bright, MRS Bull. **25**, 15 (2000).
[2]H. Kawazoe, H. Yanagi, K. Ueda, and H. Hosono, MRS Bull. **25**, 28 (2000).
[3]H. Kawazoe, M. Yasukawa, H. Hyodo, M. Kurita, H. Yanagi, and H. Hosono, Nature (London) **389**, 939 (1997).
[4]W. C. Sheets, E. Mugnier, A. Barnabe, T. J. Marks, and K. R. Poeppelmeier, Chem. Mater. **18**, 7 (2006).
[5]R. E. Stauber, J. D. Perkins, P. A. Parilla, and D. S. Ginley, Electrochem. Solid-State Lett. **2**, 654 (1999).
[6]C. H. Ong and H. Gong, Thin Solid Films **445**, 299 (2003).
[7]W. Lan, W. L. Cao, M. Zhang, X. Q. Liu, Y. Y. Wang, E. Q. Xie, and H. Yan, J. Mater. Sci. **44**, 1594 (2009).
[8]A. N. Banerjee, R. Maity, and K. K. Chattopadhyay, Mater. Lett. **58**, 10 (2004).
[9]A. Sivasankar Reddy, P. S. Reddy, S. Uthanna, and G. M. Rao, J. Mater. Sci.: Mater. Electron. **17**, 615 (2006).
[10]N. Tsuboi, Y. Takahashi, S. Kobayashi, H. Shimizu, K. Kato, and F. Kaneko, J. Phys. Chem. Solids **64**, 1671 (2003).
[11]A. N. Banerjee and K. K. Chattopadhyay, Prog. Cryst. Growth Charact. Mater. **50**, 52 (2005).
[12]A. N. Banerjee, S. Kundoo, and K. K. Chattopadhyay, Thin Solid Films **440**, 5 (2003).
[13]N. Tsuboi, Y. Itoh, J. Ogata, S. Kobayashi, H. Shimizu, K. Kato, and F. Kaneko, Jpn. J. Appl. Phys., Part 1 **46**, 351 (2007).
[14]R. S. Yu, C. J. Lu, D. C. Tasi, S. C. Liang, and F. S. Shieu, J. Electrochem. Soc. **154**, H838 (2007).
[15]P. B. Mirkarimi, M. Shinn, and S. A. Barnett, J. Vac. Sci. Technol. A **10**, 75 (1992).
[16]S. Park, B. L. Clark, D. A. Keszler, J. P. Bender, J. F. Wager, T. A. Reynolds, and G. S. Herman, Science **297**, 65 (2002).
[17]M. Ohring, *Materials Science of Thin Films*, 2nd ed. (Academic, London, 2002), pp. 216–222.
[18]K. Tonooka, K. Shimokawa, and O. Nishimura, Thin Solid Films **411**, 129 (2002).
[19]K. A. Rogers, K. P. Trumble, B. J. Dalgleish, and I. E. Reimanis, J. Am. Ceram. Soc. **77**, 2036 (1994).
[20]K. T. Jacob and C. B. Alcock, J. Am. Ceram. Soc. **58**, 192 (1975).
[21]A. N. Banerjee, C. K. Ghosh, S. Das, and K. K. Chattopadhyay, Physica B **370**, 264 (2005).
[22]R. F. Cooley and J. S. Reed, J. Am. Ceram. Soc. **55**, 395 (1972).
[23]T. Ishiguro, A. Kitazawa, N. Mizutani, and M. Kato, J. Solid State Chem. **40**, 170 (1981).
[24]B. U. Köhler and M. Jansen, Z. Anorg. Allg. Chem. **543**, 73 (1986).
[25]J. I. Pankove, *Optical Processes in Semiconductors* (Prentice-Hall, Englewood Cliffs, NJ, 1971), p. 34–85.
[26]M. Nolan, Thin Solid Films **516**, 8130 (2008).
[27]B. I. Shklovsii and A. L. Efros, *Electronic Properties of Doped Semiconductors* (Fischer, New York, 1984), Vol. 88, p. 4159.
[28]H. Yanagi, S. Inoue, K. Ueda, H. Kawazoe, H. Hosono, and N. Hamada, J. Appl. Phys. **88**, 4159 (2000).